RSC Advances

PAPER

View Article Online
View Journal | View Issue

Cite this: *RSC Adv.*, 2021, **11**, 25258

Facile fabrication of ion-imprinted Fe_3O_4/carboxymethyl cellulose magnetic biosorbent: removal and recovery properties for trivalent La ions

Long Liu,[a] Sheng Chang,[a] Yan Wang,[b] Hexiang Zhao,[a] Shuteng Wang,[a] Chengfeng Zheng,[a] Yingying Ding,[a] Shixue Ren,[a] Jiguo Zhang*[a] and Yuan-Ru Guo*[a]

An Fe_3O_4/carboxymethyl cellulose (Fe_3O_4/CMC) magnetic biosorbent was prepared using the ion-imprinting technology, where La(III) was used as the template ion. The morphology and structure of Fe_3O_4/CMC were characterized by SEM, FTIR and XRD. It is found that nano Fe_3O_4 with inverse spinel structure can distribute in CMC and endow the composite with good magnetic properties. The adsorption performance such as adsorption capacity, influence of pH and initial concentration were fully explored. The prepared Fe_3O_4/CMC is revealed to have good adsorption properties with Q_{max} of 61.5 mg g^{-1}, in line with the pseudo-second-order kinetic model. When handling the multi-ion coexistence solution of Cu(II), Ni(II) and Cd(II), Fe_3O_4/CMC shows high selective adsorption for La(III). Meanwhile, cycling experiments find that the adsorption capacity is only slightly reduced (less than 5%) after 5-time reuse. Good adsorption properties, high selectivity and easy recovery give the newly-synthesized Fe_3O_4/CMC biosorbent broad application potential in the treatment of La(III)-containing wastewater.

Received 10th May 2021
Accepted 14th July 2021

DOI: 10.1039/d1ra03647e

rsc.li/rsc-advances

Introduction

As non-renewable metal mineral resources, rare earth (RE) elements have many fascinating properties, which enable them to be widely used in agriculture,[1] optics[2] and electromagnetics[3] as well as weaponry. Due to early large-scale mining and low utilization efficiency, the reserve of REs has declined sharply. At the same time, spent REs are produced because they are frequently used and then discharged into the environment. This has a great impact on the environment on the one hand; and on the other hand it is also a waste of resources. As one of the REs, lanthanum (La) is abundant in nature. Because of its good physical and chemical properties, La has been widely utilized in many high-tech fields.[4] However, due to its toxicity, La can cause peripheral blood lymphocytes in humans once it has been discharged into the environment.[5] Therefore, the efficient recovery of La is of great significance to sustainable development as well as to environment protection/remediation.

In order to solve these problems, many methods have been exploited to remove trivalent La ion (La(III)) from wastewater, such as co-precipitation,[6] ion exchange,[7] membrane separation,[8] adsorption[9–11] as well as liquid–liquid and solid phase extraction.[12] Among them, the adsorption method has been intensively studied because of economical and effective merits. Due to this advantage, adsorption has been widely used for water treatment. With that, different adsorbents have been examined such as metal-polyphenolic nanocages,[13] organic frameworks,[14,15] MXene nanocomposites.[16–18] Of them, carbon nanotube,[19] ammonium citrate-modified biochar[4] and active carbon modified with pentaethylhexylamine[9] were applied for the removal and recovery of La(III). Although these materials showed good separation efficiency, low-cost adsorbent with high removal capacity for La(III) is still demanded.

In seeking selective adsorbent for designated elements, ion-imprinted polymers have been received a lot of attention.[20] Generally, the ion-imprinting technique covers materials of functional polymer and the target template ions, which are cross-linked by covalent or non-covalent interaction. Being eluted template ions, the ion-imprinted polymer adsorbent can be obtained, which has the memory towards the template ion. With this memory effect, the ion-imprinted polymer adsorbent can remove template ion from environment.[21–23]

As an environmental-friendly polymer, carboxymethyl cellulose (CMC) is a cheap and renewable biomass, which has good biocompatibility and degradability. CMC molecules contain a large number of hydroxyl and carboxyl groups, which can form complexes with metal ions through electrostatic attraction and

[a]*Key Laboratory of Bio-based Material Science & Technology (Ministry of Education), College of Material Science and Engineering, Northeast Forestry University, Harbin 150040, China. E-mail: 116920813@qq.com; guoyrnefu@163.com*
[b]*Harbin Center for Disease Control and Prevention, Harbin, 150056, China*

chelation, thereby effectively removing metal ions in sewage.[24–26] Thus, CMC has large adsorption capacity toward certain materials, which makes it a good candidate for the ion-imprinting polymer.[27] Some studies showed that cellulose can form magnetic adsorption materials once being combined with magnetic components. And the prepared composite had fast removal rate and easy separation property for dyes.[28]

In this work, ion-imprinted Fe_3O_4/carboxymethyl cellulose (Fe_3O_4/CMC) was prepared and La(III) was used as the template ion. The adsorption performance of Fe_3O_4/CMC for La(III) was studied. It is shown that our ion-imprinted material bears good adsorption property by means of the ion-printed technique. Meanwhile, the adsorption mechanism was hypothesised. Due to its good adsorption performance and easy separation property, environment-friendly ion-imprinted Fe_3O_4/CMC shows good application prospect for removal and recovery La(III) from the wastewater.

Results and discussion

Micro morphology of Fe_3O_4/CMC

The structure of the ion-imprinted Fe_3O_4/CMC was characterized by XRD, and results are shown in Fig. 1. From Fig. 1a, we can see that Fe_3O_4 has characteristic diffraction peaks of magnetite Fe_3O_4 standard card (JCPDS: 77-1545). The peaks at 30.1°, 35.6°, 43.3°, 53.8°, 57.1°, 62.8° and 74.5° correspond to the (200), (311), (400), (422), (511), (440) and (533) crystal planes of the inverse spinel structure of Fe_3O_4. It can be seen that there is no other peaks in the XRD pattern, indicating the pure phase of Fe_3O_4. To the pattern of Fe_3O_4/CMC, all diffraction peaks of Fe_3O_4 can be found in XRD plot, which indicated that Fe_3O_4 exits in the composite. Meanwhile, there is a broad peak around 20°, which is characteristic peak of CMC. The XRD result gave the evidence that both CMC and Fe_3O_4 coexist in composite and there is no other impurities.

Fig. 1b shows the FTIR spectra of the original CMC and Fe_3O_4/CMC. According to the IR spectrum of CMC, peak at 3365.6 cm^{-1} can be attributed to the stretching vibration absorption peak of –OH; peak at 2886.8 cm^{-1} is stretching vibration absorption peak of $-CH_2$; adsorption band of C=O in CMC located at 1716.9 cm^{-1}; adsorption bands at 1228.6 and 1012.3 cm^{-1} can be attributed to the stretching vibration absorption of –C–O–C–. Compared with the original CMC, spectrum of Fe_3O_4/CMC shows difference. It can be found that the –OH stretching vibration peak absorption is significantly reduced, and the absorption of the stretching vibration peak of –C–O–C– is significantly increased. This is probably because the acetal reaction between the –OH groups in CMC and the C=O in glutaraldehyde, which make the C=O functional groups disappear and enhance the adsorption of –C–O–C– functional groups. Moreover, adsorption peak at 564.5 cm^{-1} was found, which can be attributed to the characteristic stretching vibration of the Fe–O in Fe_3O_4. This result indicated that the cross-linked CMC successfully encapsulated the Fe_3O_4 particles.

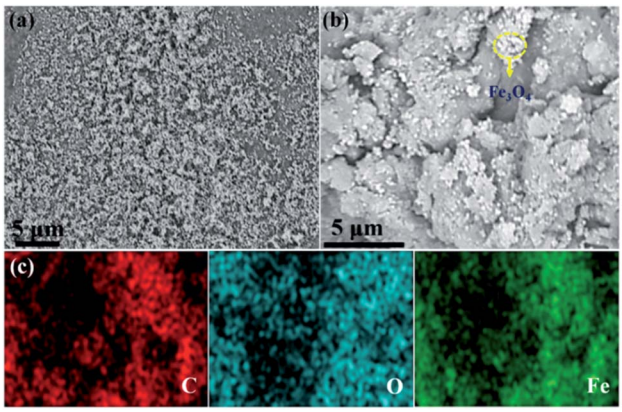

Fig. 2 SEM images of Fe_3O_4 (a), Fe_3O_4/CMC (b) and EDS mapping pictures of Fe_3O_4/CMC (c).

Fig. 2 shows the morphology of both Fe_3O_4 and Fe_3O_4/CMC, which were observed by SEM. It can be seen from Fig. 2a that Fe_3O_4 are well dispersed nanoparticles. After combined with CMC (Fig. 2b), large particles of Fe_3O_4/CMC are formed with rough surface and Fe_3O_4 nanoparticles are also found in CMC. To further prove it, the EDS was applied to Fe_3O_4/CMC and the mapping pictures were shown in Fig. 2c. From the picture, we can see that carbon, oxygen and Fe are distributed evenly in the composites, which also gave the evidence that the composite of Fe_3O_4/CMC was prepared.

The TGA analyses of both CMC and Fe_3O_4/CMC were carried out. As shown in Fig. 3, one can see that CMC itself has one-step degradation in the range of 250–430 °C, where the weight loss is 84%. The fastest degradation rate is found at 350 °C. To the composite, it degrades at the same temperature, but the fast degradation rate occurs at about 300 °C, which is higher than that of CMC. This result indicate that Fe_3O_4 is good for heat conduction. The composite reaches the balance with the weight loss of 19.4% at 550 °C. According to the TG data, the contents

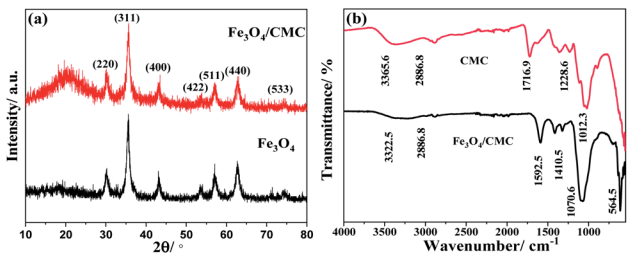

Fig. 1 XRD patterns (a) and FTIR spectra (b) of Fe_3O_4/CMC and CMC.

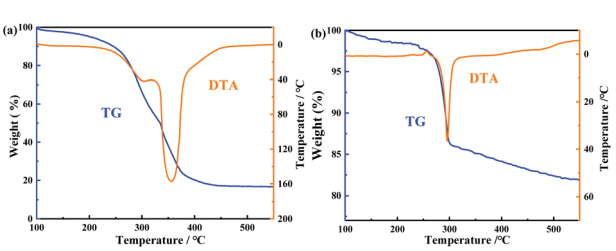

Fig. 3 The TGA and DTA of CMC and Fe_3O_4/CMC.

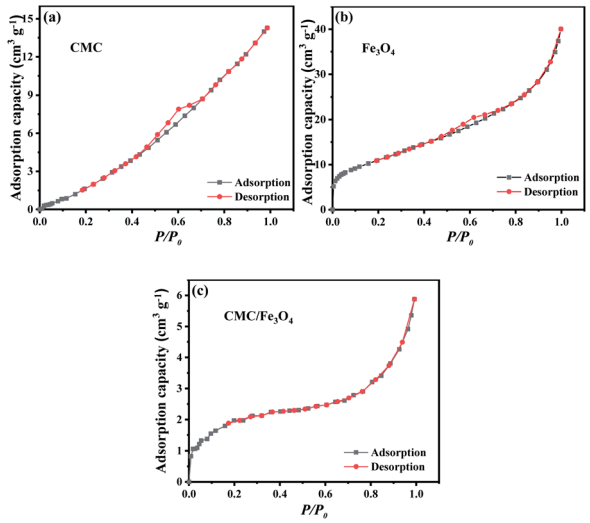

Fig. 4 Nitrogen adsorption/desorption isotherms of (a) CMC, (b) Fe_3O_4, and (c) Fe_3O_4/CMC.

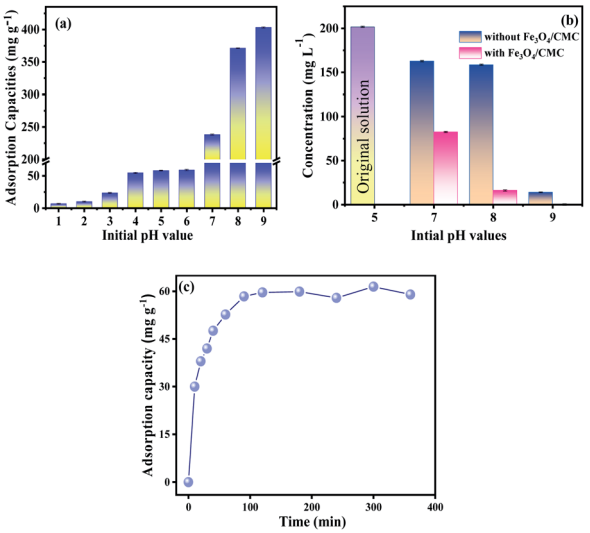

Fig. 5 The pH effect on the adsorption capacities (a) and the La(III) concentration after oscillation at high pH with and without using Fe_3O_4/CMC (b), and adsorption kinetic curve of Fe_3O_4/CMC (c).

of Fe_3O_4 and CMC in the composite are 64.6 and 35.4%, respectively.

Since the specific surface area has great impact on the adsorption capacity, BET analysis has been performed on Fe_3O_4, CMC and Fe_3O_4/CMC. The results of BET analysis are presented in Fig. 4.

From Fig. 4 and Table 1, one can note that the surface area of Fe_3O_4 is the highest due to its small particle size. The S_{BET} of CMC is 5.7 $m^2\ g^{-1}$. After coating Fe_3O_4, the S_{BET} of Fe_3O_4/CMC increases to 9.2 $m^2\ g^{-1}$. This results indicate that Fe_3O_4/CMC has not only magnetic property, which would help to recover the adsorbent, but also high specific surface area, which can improve its adsorption property.

Adsorption properties of Fe_3O_4/CMC

The adsorption property of Fe_3O_4/CMC was evaluated by templated ion of La(III). Fig. 5a shows the adsorption capacities of Fe_3O_4/CMC at different initial pH. It can be seen that the initial pH values have great influence on adsorption capacity. The adsorption capacity gradually increases as the initial pH value increases, and it reaches to 58.5 mg g^{-1} when the initial pH value is 5, further increase the pH to 6.0, the adsorption capacity increases a little. The results indicated that our composites are suitable in weak acid and neutral conditions. This is probably because H^+ in the solution at low pH is competitive with La(III) and resulted in low adsorption capacity.[29]

Table 1 Specific surface areas and pore diameters of samples[a]

Sample	S_{BET}/($m^2\ g^{-1}$)	D/nm
Fe_3O_4	38.3	6.3
CMC	5.7	7.7
Fe_3O_4/CMC	9.2	5.1

[a] S_{BET} is the specific surface area, V_p is the total pore volume, and D is the average pore diameter.

The adsorption property at high pH value has some difference. One can see that the removal capacities increase dramatically at pH 7–9. We deduce that the increase of the removal capacities is partially caused by the formation of $La(OH)_3$ precipitate.

To fully investigate the pH effect on the adsorption property, the controlled experiments at pH 7, 8 and 9 were also carried out without using Fe_3O_4/CMC. The precipitate would be found once the La(III) solution was adjusted to high pH values of 7–9. After 20 min reaction, the concentration of La(III) in solution was sampled and tested. The results are shown in Fig. 5b. It is found that the concentrations of La(III) are 168.2, and 158.7 mg L^{-1} at pH 7 and 8, respectively, which decrease compared with the original concentration of 201.7 mg L^{-1}. When further raising the pH to 9, a lot of precipitates are formed immediately. And the residual contents of La(III) is 14.08 mg L^{-1}. These indicate that almost all the La(III) ions precipitate from the solution at the high pH even without using adsorbent of Fe_3O_4/CMC.

Fig. 5c is the kinetic curve of Fe_3O_4/CMC. From the Fig. 5c, we can see that the adsorption capacity increases rapidly within 30 minutes; then it reaches equilibrium in 120 min with Q_e of 60.0 mg g^{-1}. In order to further study the adsorption mechanism, both the pseudo-first-order and pseudo-second-order kinetic models (eqn (1) and (2)) were used to fit the adsorption process.

$$\ln(Q_e - Q_t) = \ln Q_e - k_1 t \quad (1)$$

$$\frac{t}{Q_t} = \frac{1}{k_2 Q_e^2} + \frac{t}{Q_e} \quad (2)$$

Where Q_e and Q_t are the adsorption capacities (mg g^{-1}) at equilibrium and the adsorption time t, respectively; k_1 (min^{-1}) and k_2 (g mg^{-1} min^{-1}) are the pseudo-first/second-order adsorption rate constants; t is the duration of adsorption (min).

According to the data in Table 2, R^2 of the pseudo-second-order kinetic model is much higher than that of the pseudo-

Table 2 Kinetic parameters fitted by pseudo-first/second order models[a]

Pseudo-first-order			Pseudo-second-order		
k_1 (min^{-1})	R^2	$Q_{e,cal}$ (mg g^{-1})	k_2 (g mg^{-1} min^{-1})	R^2	$Q_{e,cal}$ (mg g^{-1})
1.056×10^{-2}	0.6741	23.9	1.63×10^{-3}	0.9983	61.7

[a] k_1/k_2 is first/second order rate constants, R^2 is the coefficient of determination, and $Q_{e,cal}$ is the calculated capacity at equilibrium.

first-order kinetic model, which indicated that pseudo-second-order kinetic model fits the adsorption process better. Meanwhile, the $Q_{e,cal}$ calculated by pseudo-second-order kinetic model is 61.7 mg g^{-1}, that is very close to experimental value. These results show that the adsorption process is mainly controlled by chemical reactions.[30]

The adsorption isotherm of Fe_3O_4/CMC is shown in Fig. 6a. It can be seen that the adsorption capacities gradually increase with the increase of the initial concentration of La(III). The adsorption capacity (Q_{max}) reaches the largest of 61.5 mg g^{-1} when the initial concentration of La(III)is 200 mg L^{-1}. Continue to increase the concertation of La(III), the adsorption capacity changes little. Both Freundlich and Langmuir isotherm adsorption models[10] were applied to fit the adsorption experimental data according to the eqn (3) and (4).

$$\frac{C_e}{q_e} = \frac{C_e}{q_{m,cal}} + \frac{1}{K_L q_{m,cal}} \quad (3)$$

$$\ln q_e = \ln K_F + \frac{1}{n} \ln C_e \quad (4)$$

Where C_e is the concentration of La(III) at the time of adsorption equilibrium (mg L^{-1}); q_e is the equilibrium adsorption capacity (mg g^{-1}); $q_{m,cal}$ is the calculated maximum adsorption capacity (mg g^{-1}); and K_L/K_F is the Langmuir (L mg^{-1})/Freundlich adsorption equilibrium constant (mg g^{-1}).

The fitting plots and data are shown in Fig. 6b, c and Table 3. It can be seen that the linear coefficient of determination (R^2) of the Langmuir is 0.9805, which indicating the monolayer adsorption of Fe_3O_4/CMC and La(III). The maximum adsorption capacity ($q_{m,cal}$) calculated by Langmuir fitting model is 65.3 mg g^{-1}, which is close to experimental one.[31]

Meanwhile, the R^2 obtained by fitting Freundlich model is 0.9403, indicating that the chemical adsorption undergoes: Fe_3O_4/CMC and La(III) would form chemical bondings during the adsorption.

To fully understand the adsorption mechanism, the zeta potential analyses at different pH values of Fe_3O_4/CMC were carried out. From Fig. 7a, one can see that the zeta potential of Fe_3O_4/CMC decreases as the pH in solution increases. It would reach the isoelectric point at about pH 2.5. At pH 5, the zeta potential gets to −24.5 mV. Further increasing the pH to 10, the zeta potential changes slightly. The reason for this is that there are plenty of hydrogen ions in low pH and, which can be adsorbed on the surface of the CMC and make it positively charged.

Zeta potentials of CMC, Fe_3O_4, Fe_3O_4/CMC and Fe_3O_4/CMC-La at pH 5 were also determined (Fig. 7b). Zeta potentials of CMC and Fe_3O_4 are −37.9 and 14.7 mV, respectively. To the composite, its zeta potential turns −24.5 mV. This indicates that some negative charges on the surface of CMC can be neutralized by the positive charges on the Fe_3O_4. However, the total charges on the composite surface are still retained negative, which would benefit to adsorb positive La(III) ion. After uptaken La(III), the zeta potential of Fe_3O_4/CMC-La becomes 0.43 mV. This evidences that La(III) can be adsorbed on the surface of Fe_3O_4/CMC *via* the electrostatic force.

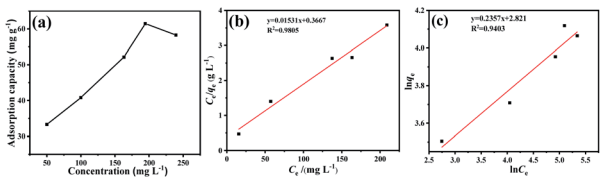

Fig. 6 The adsorption isotherm of Fe_3O_4/CMC (a), the fitting curves by Langmuir model (b) and Freundlich model (c).

Table 3 The fitted constants of adsorption isotherm by Langmuir and Freundlich models[a]

Langmuir isotherm constants			Freundlich isotherm constants		
$q_{m,cal}$ (mg g^{-1})	K_L (L mg^{-1})	R^2	K_F (mg g^{-1})	n	R^2
65.3	4.184×10^{-2}	0.9805	16.794	4.243	0.9403

[a] $q_{m,cal}$ is calculated maximum adsorption capacity. K_L is Langmuir coefficient of distribution, and K_F and n are Freundlich coefficient of distribution.

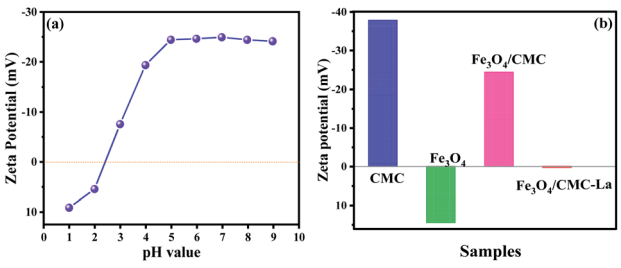

Fig. 7 The zeta potentials of (a) Fe_3O_4/CMC at *vs.* pH and (b) various samples at pH 5.

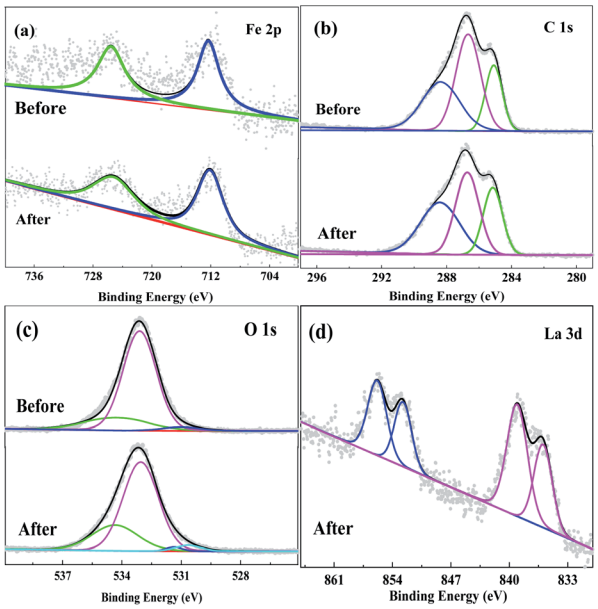

Fig. 8 XPS spectra of Fe 2P (a), C 1s (b), O 1s (c) and La 3d (d) before and after adsorption.

The XPS analysis was also applied to characterize the elemental environments of Fe_3O_4/CMC before and after adsorption. From the XPS spectra in Fig. 8, the binding energies of Fe and C show subtle difference. To XPS spectra of Fe 2p before and after adsorption (Fig. 8a), there are two peaks around 725.5 and 712.2 eV, which belong to the binding energies of Fe $2p_{1/2}$ and $2p_{3/2}$ in Fe_3O_4, respectively. The relatively weak peaks were caused by the coating layer of CMC, which blocks the signals. This also gives the evidence that Fe_3O_4 is coated by CMC. In C 1s spectra in Fig. 8b, there are three peaks can be obtained after fitting, which are located at 285.1, 286.7 and 288.4 eV. These peaks are attributed to binding energies of C–C, C–O and C=O, respectively. The binding energies of O 1s before and after adsorption are in Fig. 8c. It can be seen that three peaks are fitted to the sample of Fe_3O_4/CMC. The peak at 534.4 eV is the binding energy of C=O, the peak at 533.1 eV is the binding energy of C–O, and the binding energy of 530.7 eV is the lattice oxygen of Fe_3O_4. More importantly, another peak at 531.2 eV can be obtained for the sample after adsorption, which is assigned to the binding energy of La–O. For the sample after up-taken of La(III), four peaks are found in La 3d spectra (Fig. 8d). Ones located at 852.8 and 836.0 eV are La $3d_{3/2}$ and $3d_{5/2}$, respectively; and peaks at 856.0 and 839.2 eV are the satellite ones of La 3d. The separation energy between La $3d_{3/2}$ and $3d_{5/2}$is about 16.8 eV, indicating the existence of La(III). Both the XPS Spectra of O 1s and La 3d evidence that La(III) has been adsorbed on Fe_3O_4/CMC.

Table 5 The selective adsorption parameters of Fe_3O_4/CMC in the multi-ion coexistence solution[a]

Template ion (T) or competing ion (M)	Fe_3O_4/CMC			
	Q_e/(mg g^{-1})	C_e/(mg L^{-1})	K_d	k
La(III)	22.5	181.4	1.24×10^{-1}	—
Ni(II)	5.8	192.4	3.02×10^{-2}	4.1
Cu(II)	5.9	200.4	2.94×10^{-2}	4.2
Cd(II)	0.8	190.7	3.94×10^{-3}	31.4

[a] Q_e is the equilibrium adsorption capacity is in mg g^{-1}; C_e is equilibrium concentration of competitive adsorption is in mg L^{-1}; K_d is the partition coefficient; and k is the selectivity coefficient.

The adsorption selectivity and reuse property

In application, some other metal ions would coexist in the solution and interfere the adsorption of La(III). Thus, the competitive adsorption experiments were carried out to study the adsorption selectivity of Fe_3O_4/CMC. Ni(II), Cu(II) and Cd(II) were selected as interfering ions. In dual system, both La(III) and the competing metal ion are 200 mg L^{-1}. Table 4 shows the calculated selective adsorption parameters in the dual-ion coexistence solution. It can be seen that the distribution coefficient (K_d) to La(III) is higher than that of Ni(II)/Cu(II)/Cd(II) in the system, which means that Fe_3O_4/CMC has better adsorption performance than the competing ions when co-exiting in solution. Meanwhile, the selectivity coefficient k is larger than 1, indicating the good adsorption of selectivity for La(III).

The adsorption selectivity was also carried out in a multi-ion coexisting solution of La(III), Cu(II), Cd(II) and Ni(II). Table 5 shows the calculated selective adsorption parameters. It can be seen that the distribution coefficient K_d of Fe_3O_4/CMC to La(III) is still greater than that of competing metal ions in the multi-ion coexisting solution. However, compared with the binary ion system, the K_d is reduced to some degree. This is probably because there are three competing ions in solution, and the

Table 4 The selective adsorption parameters of Fe_3O_4/CMC in the dual-ion coexistence solution[a]

Template ion (T)/Competing ion (C)	T			C			
	Q_e (mg g^{-1})	C_e (mg L^{-1})	K_d	Q_e (mg g^{-1})	C_e (mg L^{-1})	K_d	k
La(III)/Ni(II)	46.9	154.3	0.30	4.5	188.6	0.02	12.75
La(III)/Cu(II)	32.8	171.8	0.19	16.4	190.1	0.09	2.22
La(III)/Cd(II)	44.6	162.7	0.27	2.2	199.7	0.01	25.46

[a] Q_e is the equilibrium adsorption capacity; C_e is equilibrium concentration of competitive adsorption; K_d is the partition coefficient; and k is the selectivity coefficient.

Table 6 The circulating adsorption capacity and desorption capacity of La(III) by the ion-imprinted Fe_3O_4/CMC magnetic composite[a]

	Cycles				
A	1	2	3	4	5
Q (mg g^{-1})	61.5	60.9	59.5	61.3	59.4
q_t (mg g^{-1})	45.1	46.3	45.3	46.4	46.8
	Cycles				
B	1	2	3	4	5
Q (mg g^{-1})	61.1	60.3	59.1	58.0	57.8
q_t (mg g^{-1})	60.7	59.3	58.0	57.2	56.8

[a] Q is adsorption capacity; and q_t is desorption capacity. A: water–nitric acid (100 : 1, v/v) for 90 min; B: be eluted with water–nitric acid (80 : 1, v/v) for 120 min.

total concentration of these competing metal ions is about 600 mg L^{-1}. The high concentration of competing ions make them take more sites on Fe_3O_4/CMC, which results in relative low up-taken amount for La(III). However, the k is still larger than 1, which shows Fe_3O_4/CMC still has a good selective adsorption performance for La(III) under the interference of multi-ions.

To study the reusability of Fe_3O_4/CMC, cycling experiments were carried out and 5 cycles are tested. At the end of each cycle, the Fe_3O_4/CMC-La(III) was recovered by magnet and elute before next cycle. It can be seen from Table 6 that the adsorption capacity of the Fe_3O_4/CMC are between 57.8–61.5 mg g^{-1} (Table 6). Desorption capacities depend on the condition of elution. When elute was made by water-nitric acid (100 : 1, v/v) and elution time is 90 min, desorption capacities remain between 45.1 and 46.8 mg g^{-1}. The recovery efficiency is about 70% after being re-used for 5 times as shown in Fig. 9. The relatively short time and low acid solution are not favoured by the recovery of La(III).

Since the recovery efficiency is low, desorption experiment has been carried out with the elute of water–nitric acid (80 : 1, v/v) for 120 min. The results are shown in Table 6 and Fig. 9. The recovery of La(III) can achieve almost 98% when more time and relatively strong acid eluent are used. It shows that Fe_3O_4/CMC has good durability when applied in the removal and recovery of La(III).

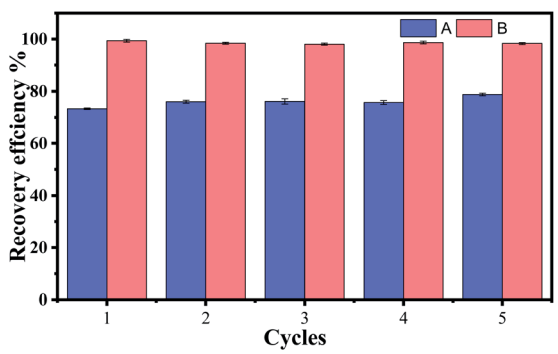

Fig. 9 The recovery efficiency when eluted with A: water–nitric acid (100 : 1, v/v) for 90 min, and B: water–nitric acid (80 : 1, v/v) for 120 min.

Conclusions

In this work, the ion-imprinted Fe_3O_4/CMC magnetic composite material was prepared with the template ion of La(III). The results of XRD, SEM and FTIR show that nano Fe_3O_4 particles distribute in CMC evenly, which enables Fe_3O_4/CMC to have good magnetic property. Adsorption performance of La(III) was fully studied and results showed that Fe_3O_4/CMC has good adsorption property for La(III). Its adsorption capacity of Q_{max} reaches 61.5 mg L^{-1}. Interfering experiments by Cu(II), Ni(II) and Cd(II) ions were also carried out, which reveals that competing ions have little effect on the adsorption of La(III). This indicates that ion-imprinted Fe_3O_4/CMC bears good selectivity for La(III). Five cycling experiments prove that Fe_3O_4/CMC has good reuse property. Facile preparation method, good selectivity and regeneration property enable Fe_3O_4/CMC to show good prospect in application of removal or recovery of La(III).

Materials and methods

Materials

Carboxymethyl cellulose (CMC, chemically pure) and glutaraldehyde (50%, chemically pure) were purchased from Tianjin Fuchen Chemical Reagent Co. Ltd; lanthanum nitrate hexahydrate ($La(NO_3)_3 \cdot 6H_2O$; 99.99%) and ethylene glycol were purchased from Shanghai Aladdin Biochemical Technology Co. Ltd and Tianjin Fuyu Fine Chemical Co. Ltd, respectively; other chemicals were purchased from Tianjin Xinbote Chemical Co. Ltd. All chemicals used in this study were analytical reagents.

Preparation of Fe_3O_4

Fe_3O_4 was prepared according to previous ref. 32. 5.0 g $FeCl_3 \cdot 6H_2O$, 2.0 g sodium citrate and 10.0 g anhydrous sodium acetate were mixed with 150 mL ethylene glycol and stirred for 5 h at room temperature. Then the mixture was transferred into 3 reaction kettles evenly and heated at 200 °C for 10 hours by hydrothermal method. The Fe_3O_4 nanoparticles were obtained after filtrated and washed in absolute ethanol and distilled water, and dried at 45 °C in a vacuum dryer.

Preparation of ion-imprinted Fe_3O_4/CMC

CMC gel was prepared by stirring mixture of 1.0 g of CMC with 50 mL distilled water for 24 h. Fe_3O_4 nanoparticles suspension was prepared by adding 0.1 g Fe_3O_4 nanoparticles into 10 mL distilled water and then oscillated for 25 min. Then the Fe_3O_4 nanoparticles suspension was added into CMC gel dropwise and continued stirring for 30 minutes to obtained mixture A. 0.1 g $La(NO_3)_3 \cdot 6H_2O$ and 2 mL glutaraldehyde were mixed with 20 mL distilled water to make mixture B. Mixed the mixture A and B to get mixture C. After 1 h stirring, mixture C was

transferred into three Petri dishes and heated at 80 °C for 4 h first and then 140 °C for 2 h. After cooling, the product was grounded and washed with absolute ethanol, dilute nitric acid and distilled water. Final product was obtained after drying at 50 °C.

Adsorption experiments

La(III) solution with an initial concentration of 200 mg L^{-1} was made by dissolving 0.3055 g $La(NO_3)_3 \cdot 6H_2O$ in 200 mL distilled water. Dilute HNO_3 or $NH_3 \cdot H{=}O$ was used to adjust the pH of La(III).

In a typical adsorption experiment, 50/100 mg Fe_3O_4/CMC was put into 100/200 mL La(III) solution and oscillated (the oscillation rate of 200 rpm) at 25 °C. During the certain time, solution was sampled and concentration of La(III) was tested by inductively coupled plasma mass spectrometer (PerkinElmer, USA, model Elan9000).

The adsorption capacity was calculated according to eqn (5).

$$Q = \frac{(C_0 - C_t)V}{m} \quad (5)$$

Where C_0 (mg L^{-1}) is the initial concentration of La(III); C_t (mg L^{-1}) is the concentration of La(III) at time t; V (L) is the volume; and m (g) is the mass of sorbent.

A multi-ion coexistence solution of La(III), Cd(II), Cu(II) and Ni(II) were prepared by the initial concentration of each ion was 200 mg L^{-1}. 50 mg Fe_3O_4/CMC was put into 50 mL of mixed solution and oscillated for 6 h. The partition coefficient (K_d) and selectivity coefficient (k) of Fe_3O_4/CMC were calculated according to the eqn (6) and (7).[33]

$$K_d = \frac{(C_0 - C_e)V}{m \times C_e} = \frac{Q_e}{C_e} \quad (6)$$

$$k = K_d(T)/K_d(M) \quad (7)$$

Where C_0 (mg L^{-1}) is the initial concentration of various ions; C_e (mg L^{-1}) is the equilibrium concentration of various ions; Q_e (mg g^{-1}) is the equilibrium adsorption capacity; $K_d(T)$ and $K_d(M)$ are the partition coefficient of template ion and the competing ion respectively; V (L) is the volume; and m (g) is the dry mass of sorbent.

Desorption experiment

To test the reuse property of Fe_3O_4/CMC, the desorption experiment was carried out. After adsorption, the Fe_3O_4/CMC-La(III) was dispersed in 100 mL nitric acid solution and oscillates at 25 °C for certain time. Then the regenerate Fe_3O_4/CMC was separate with magnet and desorption capacity was calculated according to eqn (8). Separated Fe_3O_4/CMC was washed with deionized water until it was neutral for next run.

$$q_t = c_t v/m \quad (8)$$

Where q_t (mg g^{-1}) is the desorption capacity; c_t (mg L^{-1}) is the concentration of La(III) after desorption; v (L) is the volume of nitric acid; m (g) is the mass of Fe_3O_4/CMC after adsorption.

Characterization

The Fe_3O_4/CMC was scanned and analysed with a Fourier infrared spectrometer (PerkinElmer Instruments Co., Ltd., USA) to obtain the FTIR spectra; the morphology of composite was observed with scanning electron microscope (Model TM3030, Hitachi High-Tech Co., Ltd.); an X-ray diffractometer (XRD-6100, Shimadzu Corporation) was used to explore the crystal structure of the sample.

Conflicts of interest

There are no conflicts to declare.

Acknowledgements

This work was funded by Natural Science Foundations of Heilongjiang Province (C2018006) and the National Undergraduates Training Programs of Innovation (Northeast Forestry University) (grant number 201910225280).

References

1 C. Turra, E. A. De Nadai Fernandes, M. A. Bacchi, G. A. Sarriés and A. E. L. Reyes, *Plant Soil*, 2019, **437**, 291–299.
2 Z. Huang, M. Fan and H. Tian, *J. Rare Earths*, 2020, **38**, 219–226.
3 Z. Zhu, M. Guo, X.-L. Li and J. Tang, *Coord. Chem. Rev.*, 2019, **378**, 350–364.
4 Y.-Y. Wang, H.-H. Lu, Y.-X. Liu and S.-M. Yang, *Colloids Surf., A*, 2016, **509**, 550–563.
5 W. Yongxing, W. Xiaorong and H. Zichun, *Bull. Environ. Contam. Toxicol.*, 2000, **64**, 611–616.
6 S. Saracoglu, M. Soylak, D. S. K. Peker, L. Elci, W. N. L. dos Santos, V. A. Lemos and S. L. C. Ferreira, *Anal. Chim. Acta*, 2006, **575**, 133–137.
7 C. Xiong, L. Xiaozheng and Y. Caiping, *J. Rare Earths*, 2008, **26**, 851–856.
8 Y. Zhang, B. Van der Bruggen, L. Pinoy and B. Meesschaert, *J. Membr. Sci.*, 2009, **332**, 104–112.
9 E. M. Iannicelli-Zubiani, P. Gallo Stampino, C. Cristiani and G. Dotelli, *Chem. Eng. J.*, 2018, **341**, 75–82.
10 W.-M. Yin, Y. Wang, Y.-C. Hou, Y. Sun, J.-G. Zhang, H.-L. Sun, S.-J. Li, Q.-J. Pan and Y.-R. Guo, *Chem. Eng. J.*, 2020, **401**, 125961.
11 N.-D. Zhao, Y. Wang, X.-H. Zou, W.-M. Yin, X.-Y. Wang, Y.-R. Guo and Q.-J. Pan, *Chem. Eng. J.*, 2021, **426**, 130812.
12 E. Y. Danish, H. M. Marwani, K. F. Almoslehi and E. M. Bakhsh, *Environ. Sci. Pollut. Res.*, 2020, **27**, 5408–5417.
13 L. Mei, P. Ren, Q.-y. Wu, Y.-b. Ke, J.-s. Geng, K. Liu, X.-q. Xing, Z.-w. Huang, K.-q. Hu, Y.-l. Liu, L.-y. Yuan, G. Mo, Z.-h. Wu, J. K. Gibson, Z.-f. Chai and W.-q. Shi, *J. Am. Chem. Soc.*, 2020, **142**, 16538–16545.
14 J. Yu, L. Yuan, S. Wang, J. Lan, L. Zheng, C. Xu, J. Chen, L. Wang, Z. Huang, W. Tao, Z. Liu, Z. Chai, J. K. Gibson and W. Shi, *CCS Chem.*, 2019, **1**, 286–295.

15 L. Yuan, M. Tian, J. Lan, X. Cao, X. Wang, Z. Chai, J. K. Gibson and W. Shi, *Chem. Commun.*, 2018, **54**, 370–373.
16 L. Wang, H. Song, L. Yuan, Z. Li, P. Zhang, J. K. Gibson, L. Zheng, H. Wang, Z. Chai and W. Shi, *Environmental Science & Technology*, 2019, **53**, 3739–3747.
17 L. Wang, H. Song, L. Yuan, Z. Li, Y. Zhang, J. K. Gibson, L. Zheng, Z. Chai and W. Shi, *Environmental Science & Technology*, 2018, **52**, 10748–10756.
18 P. Zhang, L. Wang, K. Du, S. Wang, Z. Huang, L. Yuan, Z. Li, H. Wang, L. Zheng, Z. Chai and W. Shi, *J. Hazard. Mater.*, 2020, **396**, 122731.
19 L. Huang, L. Liu, W. Huang, B. Zhao, Z. Shen, Y. Bao and H. Znad, *RSC Adv.*, 2021, **11**, 4751–4759.
20 M. Roushani, S. Abbasi, H. Khani and R. Sahraei, *Food Chem.*, 2015, **173**, 266–273.
21 Z. Zhou, Y. Hu, Z. Wang, H. Zhang, B. Zhang and Z. Ren, *New J. Chem.*, 2021, **45**, 9582–9590.
22 E. Liu, X. Lin, D. Zhang, W. Xu, J. Shi and Y. Hong, *New J. Chem.*, 2021, **45**, 725–734.
23 J. Li and H. Cheng, *RSC Adv.*, 2020, **10**, 43425–43431.
24 L. Song, F. Liu, C. Zhu and A. Li, *Chem. Eng. J.*, 2019, **369**, 641–651.
25 K. Manzoor, M. Ahmad, S. Ahmad and S. Ikram, *ACS Omega*, 2019, **4**, 17425–17437.
26 K. Manzoor, M. Ahmad, S. Ahmad and S. Ikram, *RSC Adv.*, 2019, **9**, 7890–7902.
27 H. N. Bhatti, Y. Safa, S. M. Yakout, O. H. Shair, M. Iqbal and A. Nazir, *Int. J. Biol. Macromol.*, 2020, **150**, 861–870.
28 B. Chen, F. Long, S. Chen, Y. Cao and X. Pan, *Chem. Eng. J.*, 2020, **385**, 123926–123937.
29 M. Ahmad, B. Zhang, J. Wang, J. Xu, K. Manzoor, S. Ahmad and S. Ikram, *Int. J. Biol. Macromol.*, 2019, **136**, 189–198.
30 X. Ao and H. Guan, *Adsorpt. Sci. Technol.*, 2017, **36**, 026361741772226.
31 J. Fu, Z. Chen, M. Wang, S. Liu, J. Zhang, J. Zhang, R. Han and Q. Xu, *Chem. Eng. J.*, 2015, **259**, 53–61.
32 S. T. Senthilkumar, R. K. Selvan, Y. S. Lee and J. S. Melo, *J. Mater. Chem. A*, 2013, **1**, 1086–1095.
33 Z. H. Sheng, L. Shao, J. J. Chen, W. J. Bao, F. B. Wang and X. H. Xia, *ACS Nano*, 2011, **5**, 4350–4358.